



RESEARCH ARTICLE

Detecting carotenoids in salt crystals: insights into biosignature detection under Mars-like proton irradiation using in situ and ex situ Raman spectroscopy

Lucas Bourmancé¹, Frédéric Foucher² , Aurélien Canizarès² and Adrienne Kish¹ 

¹Unité Molécules de Communication et Adaptation des Microorganismes (MCAM), Muséum National d'Histoire Naturelle (MNHN), CNRS, Paris, France

²CNRS, Université d'Orléans, CEMHTI UPR 3079, Orléans, France

Corresponding author: Lucas Bourmancé; Email: lucas.bourmance@gmail.com

Received: 11 December 2024; **Revised:** 04 June 2025; **Accepted:** 06 June 2025

Keywords: brines; carotenoids; halophile; *Halobacterium salinarum*; hypersaline; Mars; proton irradiation; Raman spectroscopy

Abstract

The search for biosignatures of past microbial life has promoted the interest in halophilic archaea trapped inside fluid inclusions of salt crystals. These hypersaline environments are promising targets for the preservation of microbial cell envelope biomolecules. In this study, we focused on the preservation of bacterioruberin, a carotenoid pigment found in the cell envelope of *Halobacterium salinarum*, within fluid inclusions of salt crystals mimicking early Mars environments and modern Earth. Halite (NaCl) and sylvite (KCl) crystals were subjected to Mars-like proton irradiation, and the preservation of carotenoids was assessed using in situ and ex situ Raman spectroscopy. Our findings demonstrate that Raman spectroscopy efficiently detected carotenoids within fluid inclusions in non-irradiated crystals. However, post-irradiation analyses posed great challenges due to fluorescence induced by the formation of colour centres in the crystal lattice, which suppressed the carotenoid signal. Cleavage of irradiated crystals revealed preserved carotenoid pigments beyond the radiation penetration depth, suggesting potential preservation of biomolecules in deeper inclusions within larger crystals. Furthermore, in some cases, carotenoids were detected even within fluorescent zones, suggesting extensive preservation. This study underscores the potential of Raman spectroscopy for the detection of carotenoids as biosignatures in planetary exploration contexts, particularly as a preliminary screening tool. However, it also highlights the need for optimized protocols to overcome fluorescence-related limitations. These findings contribute to the methodologies for detecting and interpreting biosignatures in salt deposits, advancing the search for possible traces of past microbial life beyond Earth.

Contents

Introduction	2
Material and methods	3
<i>Halobacterium salinarum</i> NRC-1 culture	3
Cell envelope extraction	3
Brine solutions preparation	4
Salt crystal preparation	5
X-ray diffraction (XRD)	5
Ex situ Raman spectroscopy	5
Proton irradiation and in situ Raman spectroscopy	5
Results	6

Evaporate crystal characterization by X-ray diffraction	6
Pre-irradiation measurements	7
<i>Control ex situ Raman spectroscopy</i>	7
<i>Control in situ Raman spectroscopy</i>	7
Proton irradiation	7
<i>Irradiation in situ measurements</i>	7
<i>Post-irradiation ex situ measurements</i>	10
Discussion	11
Supplementary material	12

Introduction

The search for possible traces of past microbial life on other planets requires identifying detectable biomarkers that can be preserved over geologically relevant time scales. These molecules must also be stable after exposure to radiation conditions not found on Earth. Hypersaline environments have been identified on Earth and exist, or once existed, on other planetary bodies such as Mars and icy moons like Europa (Bramble and Hand, 2024; Fairén *et al.*, 2010; Osterloo *et al.*, 2008). This has led to increasing interest in terrestrial extremophilic microorganisms living in hypersaline habitats and their preserved biomolecules. Salt crystals formed from hypersaline environments contain fluid inclusions bearing remnants of the original brine. These fluid inclusions are of particular interest for biomolecule detection due to their distinctive properties, such as low dissolved oxygen levels due to hypersalinity, high viscosity and specific ionic compositions that contribute to the preservation of biomolecules (Bourmancé *et al.*, 2025; Kish *et al.*, 2009; Ivković-Jensen and Kostić, 1997; Pernin *et al.*, 2019). Additionally, they have been suggested to be isolated from external environmental influences for geologically-relevant time scales (Brennan *et al.*, 2013; Lowenstein *et al.*, 2005), providing micro-environments with potential for preserving traces of past microbial life. Given that different salt compositions can exert stabilizing or destabilizing effects on macromolecular structures – referred to as kosmotropic (stabilizing) and chaotropic (destabilizing) effects – it is essential to examine composition of different brines effects on the preservation of potential biosignatures (Bourmancé *et al.*, 2025; Cray *et al.*, 2013; Gault and Cockell, 2021). Although hypersaline environments on Earth are largely dominated by sodium chloride, diverse salt compositions exist. This diversity is expected to be even more pronounced in extraterrestrial environments, which have unique geological histories (Stevens *et al.*, 2019; Tosca *et al.*, 2011; Ventosa and Arahall, 2009). Furthermore, fluid inclusions within a single salt crystal do not all form simultaneously, resulting in inclusions of varying compositions (Brennan *et al.*, 2013; Lowenstein *et al.*, 2005). On Earth, halophiles such as *Halobacterium salinarum* can become entrapped within halite (NaCl) fluid inclusions during evaporative processes (Jaakkola *et al.*, 2016). One of the most prominent features of *Hbt. salinarum* is the presence of a distinctive C50 carotenoid pigment, bacterioruberin, within its cell envelope (Eichler, 2019), which can act as a biosignature even after cell death. Bacterioruberin is responsible for the characteristic red-orange coloration of halophilic archaea. It serves multiple protective functions, including shielding against oxidative stress and UV radiation (Grivard *et al.*, 2022). The passive antioxidant properties of carotenoids contribute to their resistance against degradation (Ben Hamad Bouhamed *et al.*, 2024).

Raman spectroscopy is highly sensitive to carotenoids (Baqué *et al.*, 2016; Dartnell *et al.*, 2012; Edwards *et al.*, 2013; Jehlička *et al.*, 2009; Jehlička *et al.*, 2013; Marshall *et al.*, 2007; Vitek *et al.*, 2009; Winters *et al.*, 2013). Carotenoid molecules contain chromophores – chains of alternating single and double carbon bonds –capable of absorbing and emitting light through electronic transitions. They exhibit a strong resonance Raman effect when excited by green lasers, significantly enhancing the Raman signal of their conjugated π -bond structures and rendering them easily detectable even at low concentration (Jehlička *et al.*, 2013; Marshall *et al.*, 2007; Merlin, 1985).

Laboratory and portable Raman spectrometers have been used to detect carotenoids trapped within terrestrial halite crystals (Culka *et al.*, 2019; Winters *et al.*, 2013). These pigments have thus been

identified in fluid inclusions from halite crystals extracted from borehole cores collected at different depths, representing putative ages ranging from thousands to millions of years, suggesting potential long-term stability.

More generally, Raman spectroscopy is a key method for astrobiology and planetary exploration since it permits the detection and identification of both organic and mineral phases (Foucher, 2018; Edwards *et al.*, 2007; Foucher *et al.*, 2015; Marshall *et al.*, 2010). The Perseverance rover of the NASA Mars 2020 mission is equipped with two miniaturized Raman spectrometers, SHERLOC and SuperCam (Maurice *et al.*, 2021; Razzell Hollis *et al.*, 2022), and the Rosalind Franklin rover of the ESA ExoMars mission is equipped with the Raman Laser Spectrometer instrument, located within the rover (Rull *et al.*, 2017; Rull and Martínez-Frías, 2006).

Due to the low-pressure atmosphere and in the absence of a magnetic field, the surface of Mars has been continuously exposed to high-energy UVC radiation, solar energetic particle (SEP) and galactic cosmic rays (GCR). The UVC radiation (down to 190 nm) degrades organics in the first millimetres of the Martian regolith (Baqué *et al.*, 2016, 2022; Fornaro *et al.*, 2018, 2020; Patel *et al.*, 2004; Poch *et al.*, 2014; Ranjan *et al.*, 2017; Zent and McKay, 1994). While SEP and GCR are less deleterious, they may penetrate deeper, up to several metres, and thus alter organics over time in the near subsurface (Baqué *et al.*, 2017; Brandt *et al.*, 2017; Dartnell *et al.*, 2012; Foucher *et al.*, 2025; Kminek and Bada, 2006; Pavlov *et al.*, 2012). Despite continuous irradiation in such environments, brines remain of significant interest, as non-biogenic organic compounds have been identified within halite crystals originating from meteorites (Chan *et al.*, 2018). The effect of particle irradiation on organic molecules, and carotenoids in particular, has been studied before with success using different ion beam accelerators (Kminek & Bada, 2006; Pavlov *et al.*, 2012).

Here, we investigated the stability of carotenoids trapped within evaporite crystals after exposure to proton radiation, simulating up to several billion years in the near subsurface of Mars, using the light ion accelerator Pelletron at CEMHTI, CNRS, Orléans, France. The originality of these experiments is derived from the use of uncrushed material (single crystals of different salts), along with an original device permitting Raman signal collection in situ within the proton irradiation chamber (Foucher *et al.*, 2025). We were thus able to follow the decrease in the Raman signal of carotenoids, associated with the degradation processes, with the increasing proton fluence. Then, based on previous modelling, we estimate the equivalent irradiation time on Mars and show that this biosignature could be preserved over several hundred thousand years inside salt crystals in the near subsurface of Mars. Finally, we discuss some points of improvement for future experiments.

Material and methods

Halobacterium salinarum NRC-1 culture

Halobacterium salinarum NRC-1 strain was obtained from Dr. Caryn Evilia (Idaho State University). Five biological replicate cultures of *Hbt. salinarum* were inoculated in Complex Medium+ (CM+: 4.28 M NaCl, 81 mM MgSO₄·7H₂O, 27 mM KCl, 10 mM trisodium citrate·2H₂O, 1% (w/v) peptone Oxoid® LP0034, 0.5 % (v/v) 100% Glycerol, Metal trace solution: 6.3 µM FeSO₄·7H₂O, 1.5 µM ZnSO₄·7H₂O, 2.19 µM MnSO₄, 4 nM CuSO₄·5H₂O, pH adjusted to 7.4) and incubated at 42°C, 220 rpm in the dark, mimicking a buried halite environment, until they reached stationary phase (OD₆₀₀ = 1.3–1.4).

Cell envelope extraction

Cultures were harvested by centrifugation at 10,000×g for 10 min, and the cell pellet was resuspended in 10 mL of basal salt solution (BSS: CM+ without organics). Since the long-term survival of *Halobacterium salinarum* cells within fluid inclusions is uncertain, this study focused on a scenario in which the cells eventually die and undergo lysis, resulting in the release and potential preservation of

Table 1. Brine compositions. Brine M1 and M2 (based on Stevens *et al.*, 2019; Tosca *et al.*, 2011)

Brine composition (mol L ⁻¹)	Type I (Nakhla Martian meteorite)	Type II (Merridiani planum)	Control
	M1	M2	BSS
NaCl	1.27	2.27	4.28
KCl	3.78	1.33	0.27
MgCl ₂ .6H ₂ O		1.15	
MgSO ₄ .7H ₂ O		2.55	0.81
HCl		0.39	
Trisodium citrate.2H ₂ O			0.13
CaCl ₂			
KHCO ₃	2.24		
FeSO ₄ .7H ₂ O			
FeCl ₂ .4H ₂ O			
Na ₂ SO ₄			
Mg(ClO ₄) ₂			
pH	8.3	1	7.4

cell envelope fragments. Cell lysis was achieved by a single freeze/thaw cycle using liquid nitrogen. As *Hbt. salinarum* cells are highly polyploid, each sample was treated with 4 mg of DNase 1 (DN25, Merck) for 30 min at 37°C using a Tube Revolver (force 15) to remove DNA. Raw cell envelope fractions were then harvested by centrifugation 20,000×g for 2 h at 4°C and washed using three successive ultracentrifugation cycles (70.1Ti Rotor, Beckman) at 100,000×g for 30 min at 4°C with 10 mL of fresh BSS per cycle. The resulting cell envelope pellets were then resuspended in 1 mL Tris-HCl buffer, pH 7.4 (Tris buffer), and any remaining cytosolic contaminants removed using a 20–55% sucrose gradient (5% increments in Tris buffer) with centrifugation at 80,000×g for 15 h at 10°C. The red, carotenoid-bearing cell envelope fractions were collected and washed three times in Tris buffer by centrifugation at 229,600×g 4°C for 1 h. The purified cell envelope fractions were resuspended in 2 mL of Tris buffer using an ice-cold ultrasonic bath (Advantage Lab, AL-04-04) for 5 min. Proteins were quantified by bicinchoninic acid assay (BCA) (Pierce™ BCA Protein Assay Kit, ThermoFisher Scientific), with 125 µg aliquots of cell envelope lyophilized and stored at -20°C until use.

Brine solutions preparation

The brines used in this study were selected to mimic two early Mars environments as well as modern Earth, all being environments where halite is or could have formed (see Table 1) (Brennan *et al.*, 2013; Lowenstein *et al.*, 2005; Stevens *et al.*, 2019). The pH of each solution was not adjusted to preserve conditions more closely resembling the natural environment being modelled. As the brines were supersaturated, the solutions were prepared in borosilicate bottles by first adding the required salts to ultrapure (MQ®) water (MQH₂O) at approximately 20% of the final desired solution volume. The mixture was continuously stirred with a magnetic stirrer for 1 h, and then the volume was completed with MQH₂O before incubation for 5 days at 30°C to equilibrate the liquid and solid phases. Finally, each bottle was sealed with three layers of parafilm to avoid evaporation and stored in the dark at room temperature to avoid any photochemical side reactions that could alter the solutions.

Salt crystal preparation

Cell envelope extracts (500 µg) were resuspended in 5 mL of brine solutions using an ice-cold ultrasonic bath to ensure thorough homogenization. The resulting suspensions were transferred into small petri dishes (60 mm × 15 mm), which were placed inside a desiccator containing silica beads. The lids of the petri dishes were removed, and the desiccator was subsequently incubated at 37°C. As evaporation progressed, the initial crystallization at the bottom of the petri dishes was monitored, and the first crystals to form were carefully harvested. These crystals were dried and stored in a separate petri dish within a second desiccator, maintained at room temperature (Supplementary Figure 1).

X-ray diffraction (XRD)

XRD measurements were performed using a PANalytical X'Pert PRO diffractometer equipped with a Co anode X-ray tube operating at 45 kV and 40 mA. The wavelength for Co K- α radiation was used, with K- α_1 = 1.789 Å and K- α_2 = 1.793 Å. The system was configured in a θ/θ reflection geometry with a programmable divergence slit set at 0.5°. A Soller slit of 0.04 rad was applied to both the incident and diffracted beams, and a fixed 1° anti-scatter slit was used. The diffracted beam path was further filtered using an iron (Fe) β -filter of 0.016 mm thickness.

The samples were crushed to a thin powder and mounted on a Spinner PW3064 sample stage and scanned in continuous mode over a 2θ range of 5°–100° with a step size of 0.001°. A common counting time of 80 seconds per step was applied. The sample was rotated during measurement, with a revolution time of 8 seconds, to improve particle statistics. Data were collected using an X'Celerator detector operating in scanning mode, with an active length of 2.122°.

Fine calibration offsets of 0.002° and -0.014° were applied for 2θ and omega, respectively, to ensure measurement accuracy. Data collection was managed by Data Collector software version 4.1, and the instrument was controlled by X'Pert PRO software version 2.1E.

Data were analysed using HighScore Plus software. Peaks were selected based on a significance threshold of 10, and only those with an intensity of at least 1% of the strongest peak's intensity were included.

Ex situ Raman spectroscopy

High-resolution Raman spectroscopy analyses were carried out before and after irradiations using a *WITec Alpha 500RA* system, at the CEMHTI laboratory, CNRS, Orléans, France, equipped with a green laser (Nd:YAG frequency-doubled laser) of wavelength λ = 532 nm. The laser power was set to 14 mW at the sample surface. Spot analyses and Raman mapping were acquired using *Nikon E Plan* objectives of magnification 20× (numerical aperture N.A. = 0.40) or 50× (N.A. = 0.75), for which the associated laser spot size diameter at the sample surface has been measured to 2.4 and 1.16 µm, respectively (Foucher, 2022). Raman spectra were acquired using a 600 g.mm⁻¹ grating spectrometer ranging from approximately 70 to 3800 cm⁻¹ and a resolution ranging from 3 to 5 cm⁻¹. Raman maps display the bands area of the different phases obtained after spectral and spatial data processing (e.g. background subtraction, application of masks). Average spectra were obtained from the maps using mathematical threshold filters (Foucher *et al.*, 2017).

Proton irradiation and in situ Raman spectroscopy

The irradiation experiments were carried out in the microbeam line vacuum chamber of the CEMHTI Pelletron facility (<http://emir.in2p3.fr/CEMHTI>), with a 2.8 MeV proton (H⁺) beam. The beam has a 5 × 5 mm² square shape, and magnets are used to deflect the protons and to scan the sample with a Lissajous curve over an 18.5 mm diameter area. The flux at the sample surface is ca. 4 × 10¹⁰ p cm⁻² s⁻¹.

Based on (Keating *et al.*, 2005), considering that SEP protons are only delivered at their maximum fluence 3 days per year on average (i.e. during solar flares), it is possible to estimate the flux of protons at the surface of Mars to ca. $6 \text{ p cm}^{-2} \text{ s}^{-1}$. The fluence at Pelletron is thus 10^{10} times higher than on the Martian surface, permitting to simulate several hundred thousand years of irradiation in a few hours. Consequently, such experiments are only relevant for non-living organisms.

Here, it is important to note that we used a mono-energetic proton beam while the surface of Mars is exposed to a wide variety of particles, from photons to heavy ions, and at a wide energy range, from a few keV to several GeV (Keating *et al.*, 2005; Le Postolec *et al.*, 2009). Even though protons represent 91% of the GCR and 95% of the SEP (Le Postolec *et al.*, 2009; Takigawa *et al.*, 2019), and heavy ions only 1% of the GCR, the latter will induce different defects in the materials that are not considered in this study.

Material alteration under irradiation is generally studied as a function of dose, expressed in gray (Gy), 1 Gy corresponding to 1 J kg^{-1} . The total dose delivered to the sample can be expressed as follows (Foucher *et al.*, 2025):

$$D_T(\text{Gy}) = 1.602 \times 10^{-9} \times (F/\rho) \times (E/d) \quad (1)$$

With F the fluence in p cm^{-2} , ρ the density in g cm^{-3} , E the particle energy (i.e. protons in this work) in MeV and d the stopping distance of the particle in the material in millimetres. Using the SRIM software (Ziegler *et al.*, 2010), we estimate the stopping distance of the 2.8 MeV protons in salts at about $100 \text{ }\mu\text{m}$. It is important to note that, locally, the delivered dose is heterogeneous in the material; it is maximum at the Bragg's peak, located near the stopping distance of the particle (Foucher *et al.*, 2025). Nevertheless, as a first approximation, it is possible to estimate the average dose over the salt depth of $100 \text{ }\mu\text{m}$ to:

$$D = D_T/2 \quad (2)$$

In order to follow the evolution of the samples during the irradiation, an original in situ Raman device called RAMSESS (for Raman SpEctroscopy for in situ Studies) was developed (Canizarès *et al.*, 2022). Here, we used an upgraded version of this system (RAMSESS 2, see Foucher *et al.*, 2025) including a new lid for the irradiation chamber permitting the use of a new Raman probe equipped with microscope objectives, and an improved sample holder cooled down by water circulation to avoid thermal degradation of the sample by the proton beam. Due to ion luminescence, the Raman signal cannot be acquired during irradiation. The sample holder is thus alternately moved from the irradiation position (i.e. perpendicular to the proton beam) to the Raman analysis position (i.e. perpendicular to the Raman laser beam) by a rotation of 90° , then moved to the different sample positions using an (X,Y,Z) goniometer. The new Raman probe is an original device derived from the Renishaw RP10 Raman probe, equipped with a white light source and a camera for optical imaging. Raman spectra were acquired with a green laser (Nd:YAG frequency-doubled laser) of wavelength $\lambda = 532 \text{ nm}$. The laser power was set to ca. 10 mW at the sample surface and focused using a Mitutoyo objective of magnification $20\times$ (numerical aperture N.A. = 0.28) for which the associated laser spot size diameter at the sample surface has been measured to ca. $15 \text{ }\mu\text{m}$. It is connected to a Renishaw RA100 spectrometer (1800 lines/mm grating, 250 mm focal length) with a spectral resolution ranging from 3.5 cm^{-1} at 200 cm^{-1} to 1.65 cm^{-1} at 3325 cm^{-1} . A thermoelectrically cooled charge-coupled device at -50°C ensures good stability of detection.

Results

Evaporate crystal characterization by X-ray diffraction

Crystal selection during collection from the evaporating brine was based solely on appearance, with the primary criterion being resemblance to pure halite crystals, as most haloarchaea have been identified in

halite. Subsequently, X-ray diffraction analysis was employed to determine the compositional nature of the crystals collected from the three brines representing modern Earth (BSS) and different compositions from ancient Mars (M1 and M2; Supplementary Table 1).

Crystals collected from the BSS brine consisted of pure halite (NaCl). Those from the M2 brine were primarily halite with minor amounts of carnallite ($\text{KCl} \cdot \text{MgCl}_2 \cdot 6\text{H}_2\text{O}$), while crystals from the M1 brine were composed of pure sylvite (KCl). Although the M1 crystals were not halite, they were included in the study to assess compositional differences in preservation properties.

Pre-irradiation measurements

Control ex situ Raman spectroscopy

Control Raman spectra were first obtained for the crystals precipitated from the three brine solutions along with control samples of the components of the original brines as pure salts for comparison (Figure 1). These measurements were used as blank measurements to subtract from the measurements with the cell envelope containing samples. These results are aligned with the composition obtained by XRD analysis. Once this was confirmed, pre-irradiation ex situ Raman mapping of the salt crystals containing cell envelope extracts was performed to determine the distribution of carotenoids in the fluid inclusions. In all three sample types, water fluid inclusions are well observed. Interestingly, natron and epsomite were detected in the fluid inclusions in M1 and M2, respectively. Natron ($\text{NaCl}_2 \cdot 10\text{H}_2\text{O}$) may have formed from the reaction of kaliginite and halite after dissolution, which indicates secondary inclusions formed after the initial crystal growth. In BSS and M1, the presence of carotenoids was detected within the inclusions, whereas in M2, carotenoids were only detected in a few areas. Carotenoid-containing cell envelope fragments formed small aggregates of a few micrometres (Figure 2) within the inclusions. This distribution of carotenoids within the crystals was then used to target the in situ Raman system.

Control in situ Raman spectroscopy

Prior to irradiation, the in situ Raman measurements within the proton irradiation chamber confirmed that the characteristic carotenoid peaks (1513 cm^{-1} for C=C stretching, 1154 cm^{-1} for C-C stretching and 1005 cm^{-1} for the rocking motions of the methyl groups) could be clearly identified in both BSS (halite) and M1 (sylvite) crystals. However, contrary to the ex situ measurements, these peaks were not observed in the M2 (halite) crystal using the in situ Raman system.

Proton irradiation

Irradiation in situ measurements

The in situ irradiation experiment comprised 6 irradiation rounds leading to the successive total fluences of $2 \times 10^{12}\text{ p cm}^{-2}$, $6 \times 10^{12}\text{ p cm}^{-2}$, $16 \times 10^{12}\text{ p cm}^{-2}$, $26 \times 10^{12}\text{ p cm}^{-2}$, $46 \times 10^{12}\text{ p cm}^{-2}$ and $66 \times 10^{12}\text{ p cm}^{-2}$. These fluences corresponded, according to Eq. (2), to average doses of ca. $2 \times 10^4\text{ Gy}$, $6 \times 10^4\text{ Gy}$, $17 \times 10^4\text{ Gy}$, $27 \times 10^4\text{ Gy}$, $48 \times 10^4\text{ Gy}$ and $69 \times 10^4\text{ Gy}$, respectively. A final irradiation was carried out to reach a fluence of $126 \times 10^{12}\text{ p.cm}^{-2}$ ($13 \times 10^5\text{ Gy}$). As the laser spot size with RAMSESS 2 was only roughly $15\text{ }\mu\text{m}$ diameter and the optical resolution was limited, it was very difficult to localize fluid inclusions in situ, especially in the absence of transmitted light. Therefore, for each sample, the focal plane was first set on the crystal surface, and then the sample was moved in the X and Y directions to find areas with a strong Raman signal of carotenoids. The sample was then moved vertically a few micrometres below the surface in order to obtain the optimal (X,Y,Z) position associated with the maximal carotenoid signal. After each irradiation, the sample holder was adjusted by a few micrometres in the X, Y and Z directions to realign it with the optimal position. This procedure compensated for any stage misalignment caused by the rotation between the “irradiation” and “Raman”

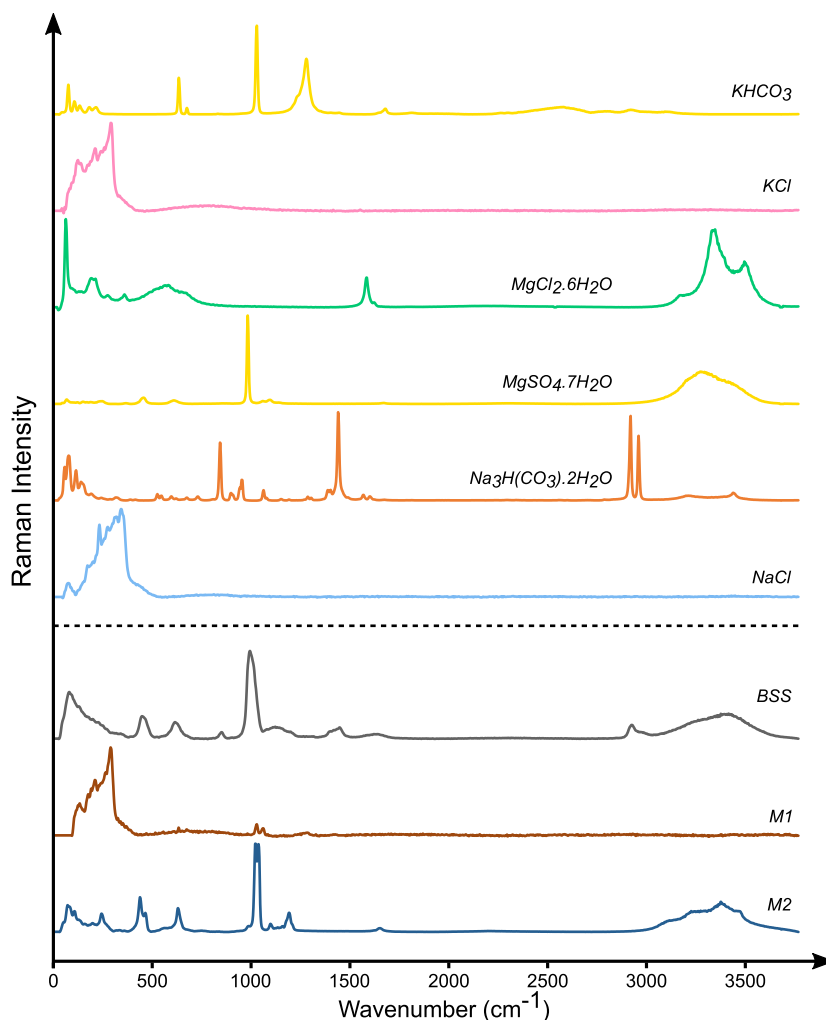


Figure 1. Raman spectra of the different salts. From top to bottom, Raman spectra of control salt crystals (above the dotted line) kaliginite (potassium bicarbonate, KHCO_3), sylvite (potassium chloride, KCl), bischofite (magnesium chloride hexahydrate, $\text{MgCl}_2 \cdot 6\text{H}_2\text{O}$), epsomite (magnesium sulphate heptahydrate, $\text{MgSO}_4 \cdot 7\text{H}_2\text{O}$), trona (trisodium citrate, $\text{Na}_3\text{H}(\text{CO}_3)_2 \cdot 2\text{H}_2\text{O}$) and halite (sodium chloride, NaCl), and below the dotted line Raman spectra of crystals formed from evaporation of the BSS, M1 and M2 crystals. These results confirmed the XRD analyses.

positions. The Raman measurement was stopped after a given number of irradiations when the carotenoid signal was no longer detectable. Additionally, for each position, the Raman spectra were normalized to their minimum value to “liberate” the signal from the focusing shift between two irradiations. Finally, the background was subtracted from the spectra using a second-order polynomial to remove the mineral fluorescence, which increased with increasing fluence.

The Raman spectrum of carotenoids acquired at the same position after each irradiation is displayed in Figure 3 for BSS and M1 crystals. For both crystals, a progressive reduction in the carotenoid signal was observed after each round of proton irradiation, leading to the complete loss of detectable signal following the final irradiation. The laser spot size and depth of field of RAMSESS 2 are approximately

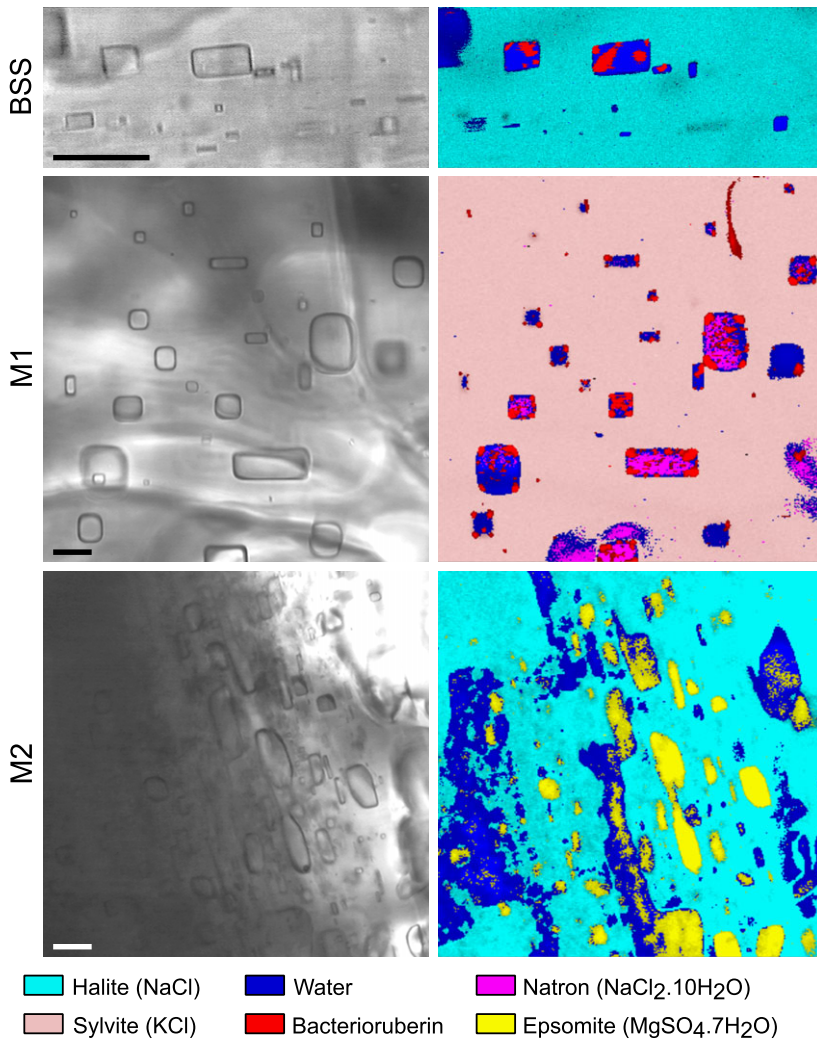


Figure 2. Raman maps of brine crystals before irradiation. Optical views (left) and associated Raman maps (right) of the different samples (scale bar 30 μm) with halite in light blue (peak area measured between 170 and 390 cm^{-1}), sylvite in pink (peak area measured between 170 and 390 cm^{-1}), water in dark blue (peak area measured between 3050 and 3650 cm^{-1}), carotenoids in red (1510 cm^{-1} peak area measured between 1460 and 1540 cm^{-1}), natron in fuchsia (1064 cm^{-1} peak area measured between 1036 and 1097 cm^{-1}) and epsomite in yellow (885 cm^{-1} peak area measured between 948 and 1030 cm^{-1}). From these observations, it was demonstrated that carotenoid-containing cell envelope fragments formed small aggregates of a few micrometres within the inclusions in BSS and M1 crystals. In the M2 crystal, however, carotenoids were only found scarcely outside inclusions (not shown here).

100 times larger than those of the ex situ system. The collected signal thus potentially corresponds to the average spectrum of several fluid inclusions, as well as carotenoids located inside or outside of inclusions. Nevertheless, this large depth of field makes it possible to obtain the average Raman spectrum over the entire irradiated depth (Foucher *et al.*, 2025).

To quantify the decrease in the Raman signal-to-noise ratio (S/N) of carotenoids with the fluence, the Raman intensity of the peak at 1513 cm^{-1} was divided by the noise measured on the 1700–1800 cm^{-1}

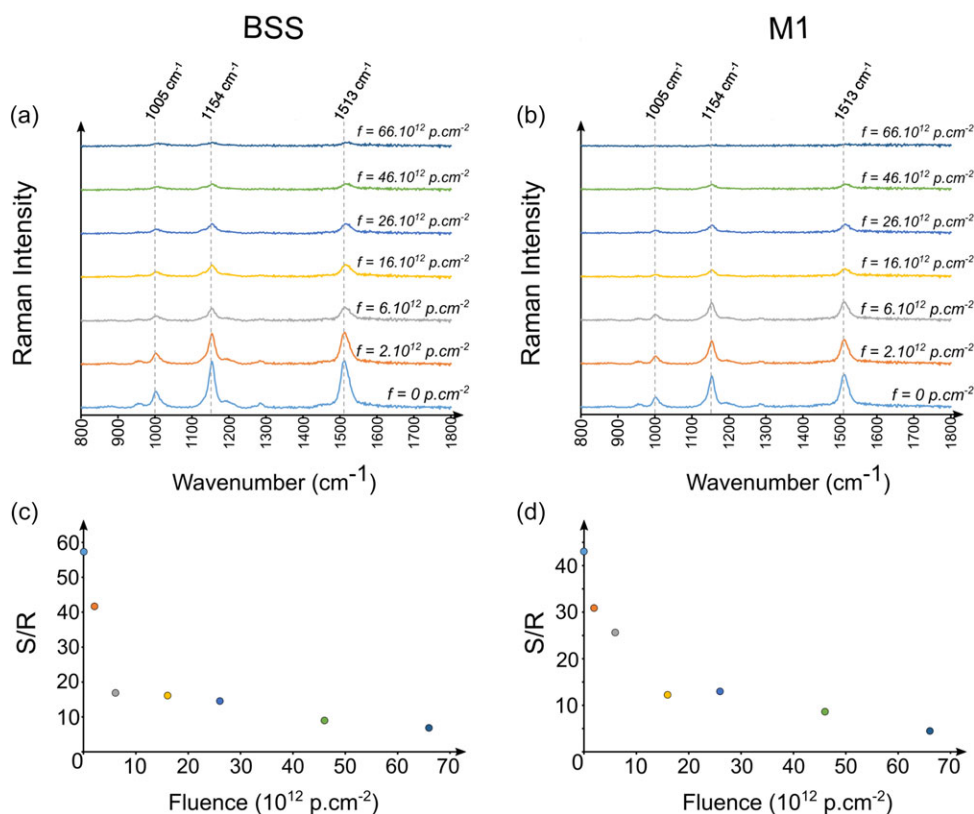


Figure 3. *In situ* Raman spectroscopy after each of the 6 rounds of proton irradiation of carotenoid pigments through the identification of C=C stretching (1513 cm^{-1}), C-C stretching (1154 cm^{-1}) and rocking motions of the methyl groups (1005 cm^{-1}). Processed Raman spectra of carotenoids acquired at the same point in (a) BSS and (b) M1 brine crystals with increasing fluence, *in situ* in the irradiation chamber, using the RAMSESS 2 device. The values of the fluence correspond to the total fluence received by the samples. The associated values of the S/N are displayed in (c) and (d), respectively. Although demonstrating the efficiency of the *in situ* set-up to detect carotenoids with fluid inclusion, signal decrease can be attributed either to degradation of the molecules or suppression of the signal due to increasing irradiation-induced fluorescence of crystals.

part of the Raman signal (i.e. a part without Raman bands). The noise was calculated using the standard deviation of the intensity, after removing of the baseline. The evolution of the S/N with increasing fluence is displayed in Figure 3c, d. It is important to note that this trend was not consistent across all fluence points, as the S/N ratio occasionally increased at higher fluences for certain points, showing variability from one measurement to another. Nevertheless, the general tendency remains the same, and a fast decrease of the S/N during the first irradiations, followed by a continuous decrease with the increasing fluence, was observed in each case.

Post-irradiation ex situ measurements

The high fluence received by the crystals (up to $126 \times 10^{12}\text{ p cm}^{-2}$) leads to an important increase in the background level associated with a strong decrease in the signal-to-noise ratio. In addition, the darkening of the crystals' surface due to the formation of colour centres under proton irradiation (Mao *et al.*, 2022; Sonnenfeld, 1995) strongly hampered the acquisition of the Raman signal several micrometres below the surface. Consequently, carotenoid signals were either undetectable or sparsely

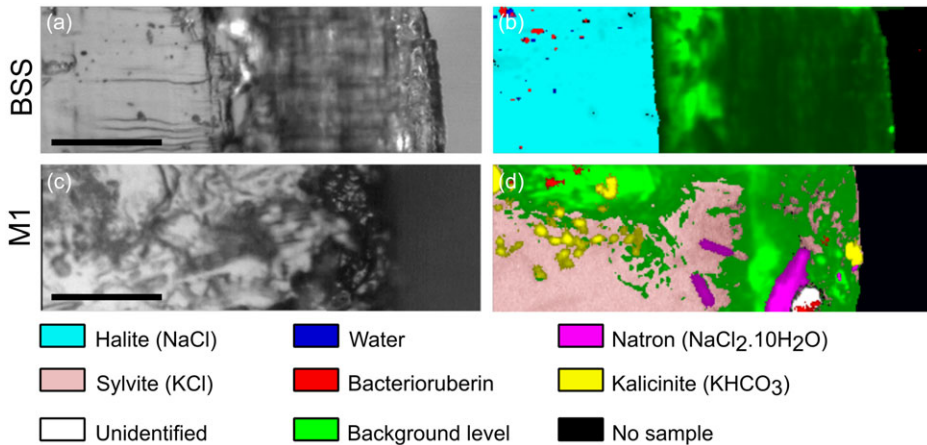


Figure 4. *Ex situ* Raman maps of cleaved brine crystals after irradiation. Optical views (panels a,b) and associated Raman maps (panels b,d) of the BSS (panels a,b) and M1 (panels c,d) brine crystals (all scale bars 30 μm). The samples were irradiated by 2.8 MeV protons and a total fluence of $126 \times 10^{12} \text{ p cm}^{-2}$; protons came from the right on the images. The irradiated surface layer is demonstrated by the increased background level displayed in green on the right side of the maps. The Raman maps display halite in light blue (peak area measured between 170 and 390 cm^{-1}), sylvite in pink (peak area measured between 170 and 390 cm^{-1}), water in dark blue (peak area measured between 3050 and 3650 cm^{-1}), carotenoids in red (1510 cm^{-1} peak area measured between 1460 and 1540 cm^{-1}), natron in fuchsia (1064 cm^{-1} peak area measured between 1036 and 1097 cm^{-1}), calicinite in yellow (1030 cm^{-1} peak area measured between 887 and 1064 cm^{-1}), the background level in green (area below the spectrum measured between 1780 and 1850 cm^{-1}), an unidentified phase in white (800 cm^{-1} peak area measured between 766 and 832 cm^{-1}) and the absence of sample in black (no spectral signal).

observed following irradiation, preventing definitive conclusions regarding the preservation of carotenoids.

The crystals were therefore cleaved, and Raman maps were acquired on the resulting sections (see Figure 4). Both M1 and BSS crystals exhibited extensive fluorescence following irradiation, with a distinct boundary marking the penetration depth of the irradiation in BSS (halite) (Figure 4b). In contrast, the fluorescence observed in M1 (sylvite) was less intense, and carotenoids were still detectable in specific locations amongst the fluorescence (Figure 4d). The absence of a detectable signal in BSS may be attributed to either the degradation of the carotenoid or to masking by the intense fluorescence of the crystal induced by proton irradiation.

Discussion

Raman spectroscopy has proven to be highly effective in detecting carotenoid pigments within the cell envelopes of haloarchaea in halite on Earth. The ExoMars rover developed by the European Space Agency (ESA) is equipped with a Raman instrument (ExoMars Raman Laser spectrometer) to search for traces of biosignatures on Mars (Veneranda *et al.*, 2020). Although not destined to analyse halite crystals, as it will land in Oxia Planum, this study aimed at demonstrating an extension of the Raman technique to study the effects of proton irradiation in other simulated Mars environments.

The brines selected in this study were computationally simulated analogues of Mars, representative of the alkaline carbonate-chloride Nakhla meteorite/Gale Crater (M1) and acidic $\text{Mg-SO}_4\text{-Cl}$ dominated Meridiani planum (M2) environments compared to the control brine BSS representative of modern Earth (Stevens *et al.*, 2019; Tosca *et al.*, 2011). Salt crystals were precipitated from these solutions by evaporation, forming halite crystals from the BSS and M2 brines and sylvite crystals from the M1 brine.

A smaller and denser form of halite was formed in the M2 solution compared those formed from the BSS brine. This is likely due to lower NaCl concentrations in the M2 brine rather than the acidic conditions as it has previously been demonstrated that pH does not influence halite growth (Jagniecki and Benison, 2010).

This study establishes a proof of concept for in situ Raman spectroscopy of salt crystals exposed to proton radiation. It is important to note that irradiation resulted in the formation of colour centres in the salt crystals, which are point defects or point defect clusters in the crystal lattice that give rise to optical absorptions (Mao *et al.*, 2022). Although this phenomenon is useful for the detection of crystals from space, it poses a significant challenge for the detection of other features within the crystals, particularly entrapped carotenoids, due to the resulting signal suppression.

However, cleaving the crystals for ex situ Raman spectroscopy proved to be an effective complementary approach. During crystallization, cell envelope fragments concentrate in fluid inclusions, which are the main source of the detected signal, despite some fragments being trapped directly into the crystal matrix. Therefore, the pigments detected were restricted to the fluid inclusions themselves. Furthermore, some carotenoids were identified within the fluorescent regions of the M1 (sylvite) crystal. This indicates good preservation in sylvite after extensive proton irradiation and highlights a distinct response compared to halite.

Based on the flux at the surface of Mars estimated from (Keating *et al.*, 2005), it is possible to estimate the dose at 1 cm below the surface of Mars to about 0.23 Gy/year (Foucher *et al.*, 2025). It is therefore possible to link the dose reached at Pelletron with a duration of irradiation on Mars. Thus, an average dose of $D = 2 \times 10^4$ Gy corresponds to ca. 90 000 terrestrial years, for example. The Raman signal of carotenoids in crystals from BSS and M1 (Nakhla meteorite/Gale Crater) brines was lost after a maximal average dose of ca. 69×10^4 Gy, corresponding to ca. 3 million years of irradiation on Mars. On the other hand, Figure 3 shows that the change in the Raman S/N ratio of carotenoids is not linear; it rapidly decreases with the increasing dose before stabilizing around 5. It is important to note here that this estimation is very rough. Indeed, alteration of materials under irradiation depends on the material density and composition. Moreover, we used a mono-energetic proton beam (2.8 MeV), while on Mars, the energy ranges from a few keV to up to several GeV. Nevertheless, these experiments showed that the Raman signal of carotenoids would potentially be detectable even after several million years of irradiation on Mars.

Taken together, these results have provided new insights into the detection of carotenoids as biosignatures in salt crystals using Raman spectroscopy:

1. Raman spectroscopy is effective for analysing carotenoids in non-irradiated salt crystals.
2. Proton irradiation induces photoluminescence of salt crystals, which complicates the detection and analysis of carotenoids trapped inside the inclusions. In that context, Raman spectroscopy could still be used as a first selection screen for the detection of carotenoid biosignatures inside salt crystals exposed to proton radiation.
3. The successful detection of carotenoids in M1 crystals even after extensive proton irradiation, equivalent to 350,000 years on Mars, is an encouraging result for biosignature preservation inside salt crystals.
4. The limitations caused by colour-induced fluorescence require that samples be collected and returned to a laboratory setting for more definitive analyses including cleaving of the crystals as a significant proportion of carotenoids could remain undetected by in situ methods.

Supplementary material

The supplementary material for this article can be found at <https://doi.org/10.1017/S1473550425100116>.

Acknowledgements. This work was supported by financing to AK from the ANR (ANR-21-CE49-0017) and the CNES Exobiology programme and to FF from the CNES Exobiology programme. We also thank the EMIR&A network for support. The authors gratefully acknowledge Thierry Sauvage, Olivier Wendling, Aurélien Bellamy, Paul Sigot and William Hate for the Pelletron platform, Caryn Evilia for the *Halobacterium* strain, Ludovic Delbes for XRD measurements and François Guyot for XRD data analysis.

Competing interests. The authors declare no competing interests.

References

- Baqué M, Backhaus T, Meeßen J, Hanke F, Böttger U, Ramkissoon N, Olsson-Francis K, Baumgärtner M, Billi D, Cassaro A, de la Torre Noetzel R, Demets R, Edwards H, Ehrenfreund P, Elsaesser A, Foing B, Foucher F, Huwe B, Joshi J, Kozyrovska N, Lasch P, Lee N, Leuko S, Onofri S, Ott S, Pacelli C, Rabbow E, Rothschild L, Schulze-Makuch D, Selbmann L, Serrano P, Szewzyk U, Verseux C, Wagner D and Westall F (2022) Biosignature stability in space enables their use for life detection on Mars. *Science Advances* 8, eabn7412.
- Baqué M, Dobrijevic M, Le Postollec A, Moreau T, Faye C, Vigier F, Incerti S, Coussot G, Caron J and Vandenabeele-Trambouze O (2017) Irradiation effects on antibody performance in the frame of biochip-based instruments development for space exploration. *International Journal of Astrobiology* 16, 82–90.
- Baqué M, Verseux C, Böttger U, Rabbow E, de Vera J-PP and Billi D (2016) Preservation of biomarkers from cyanobacteria mixed with Mars-like regolith under simulated Martian atmosphere and UV flux. *Origins of Life and Evolution of Biospheres* 46, 289–310.
- Ben Hamad Bouhamed S, Chaari M, Baati H, Zouari S and Ammar E (2024) Extreme halophilic Archaea: *Halobacterium salinarum* carotenoids characterization and antioxidant properties. *Heliyon* 10, e36832.
- Bourmancé L, Marie A, Puppo R, Brûlé S, Schaeffer P, Toupet M, Nitsche R, Elsaesser A and Kish A (2025) The salty tango of brine composition and UV photochemistry effects on *Halobacterium salinarum* cell envelope biosignature preservation. *Communications Biology* 8(1), 602.
- Bramble MS and Hand KP (2024) Spectral evidence for irradiated halite on Mars. *Scientific Reports* 14, 38448458.
- Brandt A, Meeßen J, Jänicke RU, Raguse M and Ott S (2017) Simulated space radiation: Impact of four different types of high-dose ionizing radiation on the lichen *Xanthoria elegans*. *Astrobiology* 17(2), 136–144.
- Brennan ST, Lowenstein TK and Cendon DI (2013) The major-ion composition of Cenozoic seawater: the past 36 million years from fluid inclusions in marine halite. *American Journal of Science* 313, 713–775.
- Canizarès A, Foucher F, Baqué M, de Vera JP, Sauvage T, Wendling O, Bellamy A, Sigot P, Georgelin T, Simon P and Westall F (2022). In situ Raman spectroscopy monitoring of material changes during proton irradiation. *Applied Spectroscopy* 76, 723–729.
- Chan QHS, Zolensky ME, Kebukawa Y, Fries M, Ito M, Steele A, Rahman Z, Nakato A, Kilcoyne ALD, Suga H, Takahashi Y, Takeichi Y and Mase K (2018). Organic matter in extraterrestrial water-bearing salt crystals. *Science Advances* 4, 29349297.
- Cray JA, Russell JT, Timson DJ, Singhal RS and Hallsworth JE (2013). A universal measure of chaotropy and kosmotropy. *Environmental Microbiology* 15, 287–296.
- Culka A, Košek F, Oren A, Mana L and Jehlička J (2019). Detection of carotenoids of halophilic prokaryotes in solid inclusions inside laboratory-grown chloride and sulfate crystals using a portable Raman spectrometer: applications for Mars exploration. *FEMS Microbiology Letters* 366, 31804687.
- Dartnell LR, Page K, Jorge-Villar SE, Wright G, Munshi T, Scowen IJ, Ward JM and Edwards HG (2012) Destruction of Raman biosignatures by ionising radiation and the implications for life detection on Mars. *Analytical and Bioanalytical Chemistry* 403, 131–144.
- Edwards HG, Hutchinson IB, Ingleby R, Parnell J, Vitek P and Jehlička J (2013). Raman spectroscopic analysis of geological and biogeological specimens of relevance to the ExoMars mission. *Astrobiology* 13(6), 543–549.
- Edwards HGM, Jorge Villar SE, Pullan D, Hargreaves MD, Hofmann BA and Westall F (2007) Morphological biosignatures from relict fossilised sedimentary geological specimens: a Raman spectroscopic study. *Journal of Raman Spectroscopy* 38, 1352–1361.
- Eichler J (2019) *Halobacterium salinarum*. *Trends in Microbiology* 27, 651–652.
- Fairén AG, Davila AF, Lim D, Bramall N, Bonaccorsi R, Zavaleta J, Uceda ER, Stoker C, Wierzechos J, Dohm JM, Amils R, Andersen D and McKay CP (2010) Astrobiology through the ages of Mars: the study of terrestrial analogues to understand the habitability of Mars. *Astrobiology* 10(8), 821–843.
- Fornaro T, Boosman A, Brucato JR, ten Kate IL, Siljeström S, Poggiali G, Steele A and Hazen RM (2018) UV irradiation of biomarkers adsorbed on minerals under Martian-like conditions: hints for life detection on Mars. *Icarus* 313, 38–60.
- Fornaro T, Brucato JR, Poggiali G, Corazzi MA, Biczysko M, Jaber M, Foustoukos DI, Hazen RM and Steele A (2020) UV irradiation and near infrared characterization of laboratory Mars soil analog samples. *Frontiers in Astronomy and Space Sciences* 7, 2296–987X.
- Foucher F (2018) Detection of biosignatures using Raman spectroscopy. In Cavalazzi B and Westall F (eds), *Biosignatures for Astrobiology*. Advances in Astrobiology and Biogeophysics. Cham: Springer, pp. 267–282.
- Foucher F (2022) Influence of laser shape on thermal increase during micro-Raman spectroscopy analyses. *Journal of Raman Spectroscopy* 53, 664–676.

- Foucher F, Ammar MR and Westall F (2015) Revealing the biotic origin of silicified Precambrian carbonaceous microstructures using Raman spectroscopic mapping, a potential method for the detection of microfossils on Mars. *Journal of Raman Spectroscopy* **46**, 873–879.
- Foucher F, Baqué M, Canizarès A, Martellotti R, de Vera J-PP, Sauvage T, Sigot P, Wendling O, Bellamy A, Hate W and Westall F (2025) Degradation of beta-carotene under mineral layers during proton irradiation monitored in situ by Raman spectroscopy. *Icarus* **441**, 116674.
- Foucher F, Guimbretière G, Bost N and Westall F (2017) Petrographical and mineralogical applications of Raman mapping. In *Raman Spectroscopy Applications*. IntechOpen, pp. 163–180.
- Gault S and Cockell CS (2021) Perchlorate salts exert a dominant, deleterious effect on the structure, stability, and activity of α -chymotrypsin. *Astrobiology* **21**(4), 405–412.
- Grivard A, Goubet I, Duarte Filho LMS, Thiéry V, Chevalier S, de Oliveira-Junior RG, El Aouad N, Guedes da Silva Almeida JR, Sitarek P, Quintans-Junior LJ, Grougnet R, Agogué H and Picot L (2022) Archaea carotenoids: natural pigments with unexplored innovative potential. *Marine Drugs* **20**(8), 524.
- Ivković-Jensen MM and Kostić NM (1997) Effects of viscosity and temperature on the kinetics of the electron-transfer reaction between the triplet state of zinc cytochrome c and cupriplastocyanin. *Biochemistry* **36**, 9201962.
- Jaakkola ST, Ravaniti JJ, Oksanen HM and Bamford DH (2016) Buried alive: microbes from ancient halite. *Trends in Microbiology* **24**, 148–160.
- Jagniecki EA and Benison KC (2010) Criteria for the recognition of acid-precipitated halite. *Sedimentology* **57**, 273–292.
- Jehlička J, Edwards HGM and Oren A (2013) Bacterioruberin and salinixanthin carotenoids of extremely halophilic Archaea and Bacteria: A Raman spectroscopic study. *Spectrochimica Acta Part A: Molecular and Biomolecular Spectroscopy* **106**, 99–103.
- Jehlička J, Edwards HGM and Vítek P (2009) Assessment of Raman spectroscopy as a tool for the non-destructive identification of organic minerals and biomolecules for Mars studies. *Planetary and Space Science* **57**, 606–613.
- Keating A, Mohammadzadeh A, Nieminen P, Maia D, Coutinho S, Evans H, Pimenta M, Huot J-P and Daly E (2005) A model for Mars radiation environment characterization. *IEEE Transactions on Nuclear Science* **52**, 2287–2293.
- Kish A, Kirkali G, Robinson C, Rosenblatt R, Jaruga P, Dizdaroglu M and DiRuggiero J (2009) Salt shield: intracellular salts provide cellular protection against ionizing radiation in the halophilic archaeon *Halobacterium salinarum* NRC-1. *Environmental Microbiology* **11**, 1066–1078.
- Kminek G and Bada JL (2006) The effect of ionizing radiation on the preservation of amino acids on Mars. *Earth and Planetary Science Letters* **245**, 1–5.
- Le Postollec A, Incerti S, Dobrijevic M, Desorgher L, Santin G, Moretto P, Vandenabeele-Trambouze O, Coussot G, Dartnell L and Nieminen P (2009) Monte Carlo simulation of the radiation environment encountered by a biochip during a space mission to Mars. *Astrobiology* **9**(3), 311–323.
- Lowenstein TK, Timofeeff MN, Kovalevych VM and Horita J (2005) The major-ion composition of Permian seawater. *Geochimica et Cosmochimica Acta* **69**, 1701–1719.
- Mao W, Fu X, Wu Z, Zhang J, Ling Z and Li B (2022) The color centers in halite induced by Martian dust activities. *Earth and Planetary Science Letters* **578**, 117302.
- Marshall CP, Edwards HGM and Jehlička J (2010) Understanding the application of Raman spectroscopy to the detection of traces of life. *Astrobiology* **10**(2), 229–243.
- Marshall CP, Leuko S, Coyle CM, Walter MR, Burns BP and Neilan BA (2007) Carotenoid analysis of halophilic archaea by resonance Raman spectroscopy. *Astrobiology* **7**(4), 631–643.
- Maurice S, Wiens RC, Bernardi P, Caïs P, Robinson S, Nelson T, Gasnault O, Reess J-M, Deleuze M, Rull F, Manrique J-A, Abbaki S, Anderson RB, André Y, Angel SM, Arana G, Battault T, Beck P, Benzerara K, Bernard S, Berthias J-P, Beyssac O, Bonafous M, Bousquet B, Boutillier M, Cadu A, Castro K, Chapron F, Chide B, Clark K, Clavé E, Clegg S, Cloutis E, Collin C, Cordoba EC, Cousin A, Dameury J-C, D'Anna W, Daydou Y, Debus A, Deflores L, Dehouck E, Delapp D, De Los Santos G, Donny C, Doressoundiram A, Dromart G, Dubois B, Dufour A, Dupieux M, Egan M, Ervin J, Fabre C, Fau A, Fischer W, Forni O, Fouchet T, Frydenvang J, Gauffre S, Gauthier M, Gharakanian V, Gilard O, Gontijo I, Gonzalez R, Granena D, Grotzinger J, Hassen-Khodja R, Heim M, Hello Y, Hervet G, Humeau O, Jacob X, Jacquino D, Johnson JR, Kouach D, Lacombe G, Lanza N, Lapauw L, Laserna J, Lasue J, Le Deit L, Le Mouélic S, Le Comte E, Lee Q-M, Legett C IV, Leveille R, Lewin E, Leyrat C, Lopez-Reyes G, Lorenz R, Lucero B, Madariaga JM, Madsen S, Madsen M, Mangold N, Manni F, Mariscal J-F, Martinez-Frias J, Mathieu K, Mathon R, McCabe KP, McConnochie T, McLennan SM, Mekki J, Melikechi N, Meslin P-Y, Micheau Y, Michel Y, Michel JM, Mimoun D, Misra A, Montagnac G, Montaron C, Montmessin F, Moros J, Mousset V, Morizet Y, Murdoch N, Newell RT, Newsom H, Nguyen Tuong N, Ollila AM, Orttner G, Oudda L, Pares L, Parisot J, Parot Y, Pérez R, Pheav D, Picot L, Pilleri P, Pilonget C, Pinet P, Pont G, Poulet F, Quantin-Nataf C, Quartier B, Rambaud D, Rapin W, Romano P, Roucayrol L, Royer C, Ruellan M, Sandoval BF, Sautter V, Schoppers MJ, Schröder S, Seran H-C, Sharma SK, Sobron P, Sodki M, Sournac A, Sridhar V, Standarovsky D, Storms S, Striebig N, Tatat M, Toplis M, Torre-Fdez I, Toulemont N, Velasco C, Veneranda M, Venhaus D, Virmontois C, Viso M, Willis P and Wong KW (2021) The SuperCam instrument suite on the Mars 2020 rover: science objectives and mast-unit description. *Space Science Reviews* **217**, 47.
- Merlin JC (1985) Resonance Raman spectroscopy of carotenoids and carotenoid-containing systems. *Pure and Applied Chemistry* **57**, 785–792.
- Osterloo MM, Hamilton VE, Bandfield JL, Glotch TD, Baldrige AM, Christensen PR, Tornabene LL and Anderson FS (2008) Chloride-bearing materials in the southern highlands of Mars. *Science* **319**, 1651–1654.

- Patel MR, Bérces A, Kerékgyártó T, Rontó G, Lammer H and Zarenecki JC (2004) Annual solar UV exposure and biological effective dose rates on the Martian surface. *Advances in Space Research* **33**, 1247–1252.
- Pavlov AA, Vasilyev G, Ostryakov VM, Pavlov AK and Mahaffy P (2012) Degradation of organic molecules in the shallow subsurface of Mars due to irradiation by cosmic rays. *Geophysical Research Letters* **39**, L13202.
- Pernin A, Bosc V, Soto P, Le Roux E and Maillard M-N (2019) Lipid oxidation in oil-in-water emulsions rich in omega-3: effect of aqueous phase viscosity, emulsifiers, and antioxidants. *European Journal of Lipid Science and Technology* **121**, 1800462.
- Poch O, Kaci S, Stalport F, Szopa C and Coll P (2014) Laboratory insights into the chemical and kinetic evolution of several organic molecules under simulated Mars surface UV radiation conditions. *Icarus* **242**, 50–63.
- Ranjan S, Wordsworth R and Sasselov DD (2017) Atmospheric constraints on the surface UV environment of Mars at 3.9 Ga relevant to prebiotic chemistry. *Astrobiology* **17**(8), 687–708.
- Razzell Hollis J, Moore KR, Sharma S, Beegle L, Grotzinger JP, Allwood A, Abbey W, Bhartia R, Brown AJ, Clark B, Cloutis E, Corpolongo A, Henneke J, Hickman-Lewis K, Hurowitz JA, Jones MWM, Liu Y, Martinez-Frías J, Murphy A, Pedersen DAK, Shkolyar S, Siljeström S, Steele A, Tice M, Treiman A, Uckert K, VanBommel S and Yanchilina A (2022) The power of paired proximity science observations: co-located data from SHERLOC and PIXL on Mars. *Icarus* **387**, 115179.
- Rull F and Martínez-Frías J (2006) Raman spectroscopy goes to Mars. *Spectroscopy Europe* **18**(1), 18–21.
- Rull F, Maurice S, Hutchinson I and Moral AG (2017) The Raman laser spectrometer for the exoMars rover mission to Mars. *Astrobiology* **17**(6–7), 627–654.
- Sonnenfeld P (1995) The color of rock salt—a review. *Sedimentary Geology* **94**, 267–276.
- Stevens AH, Childers D, Fox-Powell M, Nicholson N, Jhoti E and Cockell CS (2019) Growth, viability, and death of planktonic and biofilm *Sphingomonas desiccabilis* in simulated Martian brines. *Astrobiology* **19**(1), 87–98.
- Takigawa A, Asada Y, Nakauchi Y, Matsumoto T, Tsuchiyama A, Abe M and Watanabe N (2019) H⁺ ion irradiation experiments of enstatite: space weathering by solar wind. In 82nd Annual Meeting of The Meteoritical Society, p. 6331.
- Tosca NJ, McLennan SM, Lamb MP and Grotzinger JP (2011) Physicochemical properties of concentrated Martian surface waters. *Journal of Geophysical Research: Planets* **116**, E05004.
- Veneranda M, Lopez-Reyes G, Manrique-Martínez JA, Sanz-Arranz A, Lalla E, Konstantinidis M, Moral A, Medina J and Rull F (2020) ExoMars Raman Laser Spectrometer (RLS): development of chemometric tools to classify ultramafic igneous rocks on Mars. *Scientific Reports* **10**, 16954.
- Ventosa A and Arahall DR (2009) Physico-chemical characteristics of hypersaline environments and their biodiversity. In *Extremophiles II*, pp. 247–262.
- Vítek P, Osterrothová K and Jehlička J (2009) Beta-carotene—a possible biomarker in the Martian evaporitic environment: Raman micro-spectroscopic study. *Planetary and Space Science* **57**, 454–459.
- Winters YD, Lowenstein TK and Timofeeff MN (2013) Identification of carotenoids in ancient salt from Death Valley, Saline Valley, and Searles Lake, California, using laser Raman spectroscopy. *Astrobiology* **13**(11), 1065–1080.
- Zent AP and McKay CP (1994) The chemical reactivity of the Martian soil and implications for future missions. *Icarus* **108**, 146–157.
- Ziegler JF, Ziegler MD and Biersack JP (2010) SRIM – the stopping and range of ions in matter (2010). *Nuclear Instruments and Methods in Physics Research Section B: Beam Interactions with Materials and Atoms* **268**(11), 1818–1823